Proton relaxometry of tree leaves at hypogeomagnetic fields

Anne M. Fabricant[1,2]*, Piotr Put[3] and Danila A. Barskiy[1,2]*

[1]Institute of Physics, Johannes Gutenberg University of Mainz, Mainz, Germany, [2]Helmholtz Institute Mainz, GSI Helmholtzzentrum für Schwerionenforschung, Darmstadt, Germany, [3]Faculty of Physics, Astronomy and Applied Computer Science, Jagiellonian University in Kraków, Kraków, Poland

We report on a cross-species proton-relaxometry study in *ex vivo* tree leaves using nuclear magnetic resonance (NMR) at 7µT. Apart from the intrinsic interest of probing nuclear-spin relaxation in biological tissues at magnetic fields below Earth field, our setup enables comparative analysis of plant water dynamics without the use of expensive commercial spectrometers. In this work, we focus on leaves from common Eurasian evergreen and deciduous tree families: Pinaceae (pine, spruce), Taxaceae (yew), Betulaceae (hazel), Prunus (cherry), and Fagaceae (beech, oak). Using a nondestructive protocol, we measure their effective proton T_2 relaxation times as well as track the evolution of water content associated with leaf dehydration. Newly developed "gradiometric quadrature" detection and data-processing techniques are applied in order to increase the signal-to-noise ratio (SNR) of the relatively weak measured signals. We find that while measured relaxation times do not vary significantly among tree genera, they tend to increase as leaves dehydrate. Such experimental modalities may have particular relevance for future drought-stress research in ecology, agriculture, and space exploration.

KEYWORDS

nuclear magnetic resonance, relaxometry, atomic magnetometry, ultralow field, leaf water content, tree, drought stress, proton relaxometry of tree leaves at hypogeomagnetic fields

1 Introduction

The essential problem of measuring water content and dynamics in plants may seem simple enough. To this day, however, the water-monitoring toolbox remains surprisingly limited, especially where nondestructive techniques are concerned. A standard approach involves desiccating harvested plant organs and comparing their fresh and dry weights (Schnyder and Baum, 1992; Sala et al., 2007; Saura-Mas and Lloret, 2007; Huang et al., 2020). In recent years, proton (^{1}H) nuclear magnetic resonance (NMR) has emerged as a promising alternative technique, due to its sensitivity to water protons. ^{1}H NMR has found a number of plant-related applications—including measurement of water content in lumber wood (Araujo et al., 1992), investigation of moisture stress in agricultural seeds

(Krishnan et al., 2014; Unal et al., 2020), and characterization of microbial interactions in soil (Jaeger et al., 2006). Techniques based on proton relaxometry are now particularly relevant within food science (Musse et al., 2010; Khan et al., 2016; Ates et al., 2021), where magnetic resonance imaging (MRI) is also employed (As and van Duynhoven, 2013). However, commercially available NMR spectrometers typically do not have suitable geometries for measurement of intact plants or plant organs.

Leaves are arguably the most critical actor in the plant water cycle, given that a majority of transpiration and systemic water loss occurs there. Despite this, the use of proton NMR in leaf water studies is far from mainstream, although some relaxometry work has been carried out with low-field benchtop spectrometers. Notably, relaxometry of senescing rapeseed leaf pieces (excised discs) at 20MHz was investigated using a Carr-Purcell-Meiboom-Gill (CPMG) protocol, indicating an increase in some T_2 (spin-spin relaxation time, also known as coherence time) components in older leaves (Musse et al., 2013; Musse et al., 2017). A similar study at 20MHz demonstrated the utility of T_2 relaxation for phenotyping and detection of water stress in excised leaves of young potted tobacco plants (Sorin et al., 2018). At high field, proton T_2 relaxometry was applied to structural water studies in maple leaves (McCain, 1995). In addition, high-field solid-state proton NMR was shown to be effective for studying relaxation properties of dried leaves and leaf litter even when little water is present, by revealing the molecular fingerprint of plant metabolites and biopolymers (Berns et al., 2011).

The flexibility and portability of low-field NMR—loosely defined as corresponding to magnetic fields ranging from Earth field up to a few tesla, above which superconducting or hybrid superconducting/electromagnets would be required—also offers potential for taking devices directly into the field, forest, or greenhouse. One major example is the realization of *in vivo* and *ex vivo* water-proton relaxometry of intact leaves from potted agricultural plants, as well as wild shrubs and oak and poplar trees, using a unilateral 18MHz spectrometer (Capitani et al., 2009). Currently, noncommercial low-field relaxometers are being developed which enable portable *in vivo* measurement of even larger plant leaves and organs (Windt et al., 2021). Such devices complement other novel non-NMR modalities for nondestructive monitoring of leaf water potentials, e.g. nanobiosensors (Jain et al., 2021). In trees, water transport in living tree trunks and branches has been studied using custom low-field MRI and NMR devices (Nagata et al., 2016; Malone et al., 2016).

In traditional NMR systems based on inductive detection, the tradeoff between portability and achievable signal-to-noise ratio (SNR) limits how low of a magnetic field can be reasonably used for measurement of intact biological systems, where signal strengths tend to be relatively weak. It has been shown theoretically that below proton resonance frequencies of around 50MHz, detection using atomic (optically pumped) magnetometers can offer better intrinsic sensitivity than that attainable with inductive pickup coils (Savukov et al., 2007). The atomic-magnetometry detection modality has been instrumental in the subfield of zero-to-ultralow-field (ZULF) NMR (Blanchard et al., 2021; Tayler et al., 2017; Put et al., 2021; Tayler et al., 2018; Bodenstedt et al., 2021),

where ULF is commonly used in literature to refer to fields below the geomagnetic (Earth) field of tens of microtesla, such that magnetic shielding or active field cancellation is required. Due to varying definitions of ULF by different authors, some absolute (Hartwig et al., 2013) and others referenced to the spin system under study—e.g., J-coupling between spins dominates Zeeman interactions with the external field (Blanchard and Budker, 2016)—we choose instead to use the unambiguous term "hypogeomagnetic" in this publication. The hypogeomagnetic regime has already been used for direct detection of biomagnetic fields produced by plant electrical activity, including action potentials and wounding potentials (Trontelj et al., 1994; Jazbinsek et al., 2000; Fabricant et al., 2021); however, according to our understanding, NMR signals originating from plants have not yet been explored in this regime.

In addition to the fundamental question of how proton relaxation properties behave at hypogeomagnetic fields, the regime is interesting from a practical NMR standpoint, due to the low cost, portability, and low energy consumption of experimental components. Although NMR detection using superconducting-quantum-interference-device (SQUID) magnetometers (Hartwig et al., 2013; Espy et al., 2013) offers comparable sensitivity to atomic magnetometers at hypogeomagnetic fields (as well as a larger frequency bandwidth), the need for bulky cryogenic cooling limits the applicability of SQUID-based devices. The smaller footprint of atomic magnetometers also allows placement of multiple sensors around a sample, rather than in a single detection plane.

To our knowledge, the work reported here represents the broadest cross-species NMR-relaxation study of tree leaves at any magnetic field, and the first to incorporate both evergreen and deciduous varieties. Through systematic nondestructive measurement of intact leaves from seven different tree genera—spruce, pine, yew, hazel, cherry, beech, and oak—we endeavored to investigate variation in water-proton signals and relaxation times among genera. In focused studies of spruce and oak samples, we also sought to track the evolution of these parameters as a function of leaf dehydration. While relative proton signal correlates with wet mass upon dehydration, T_2 times tend to increase, indicating the possible presence of compartmentalized water reservoirs with higher water mobility surviving upon dehydration. We note that leaves and other plant tissues contain pools of both free and bound water; our approach is expected to mainly target free and loosely bound water protons. More strongly bound water protons, such as those contained in cell walls, tend to have much shorter T_2 times which would require a selective technique such as time-domain (TD) NMR to resolve (Khan et al., 2016; Windt et al., 2021).

2 Materials and methods

2.1 Relaxometry setup

Our gradiometric quadrature detection scheme is shown in Figure 1A, where two commercially available dual-axis vector magnetometers (Osborne et al., 2018) are placed orthogonally in the *x-y* plane. If the sensors, denoted 1 and 2, are positioned
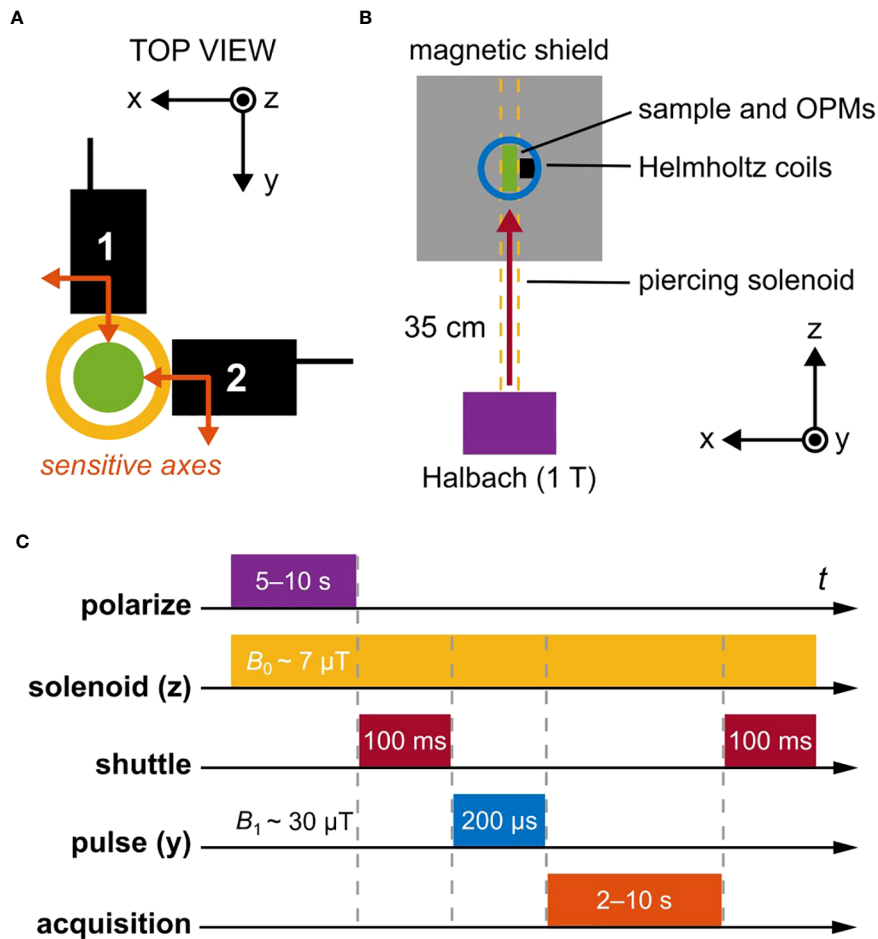
FIGURE 1
Schematic overview of the relaxometry experiment. **(A)** A pair of magnetometers (QuSpin QZFM Gen-2; sensing volume 4 × 4 × 4mm³, Rb vapor cell), each sensitive along two orthogonal axes indicated with orange arrows, are oriented in the *x-y* plane. The center of sensing volume is located 6.5mm from the tip of the sensor housing (black boxes). Samples to be measured are enclosed in a 2mL glass vial with outer diameter 11.6mm (green circle), located in a plexiglass tube around which a solenoid is wound (yellow circle). The outer diameter of the solenoid is approximately 22mm, so that the minimum offset distance of the sensing volume from the center of the sample is 17.5mm. **(B)** Nuclear spins are first thermally polarized in a 1T permanent magnet (Halbach array) before being mechanically shuttled into a magnetically shielded environment. There, three orthogonal pairs of Helmholtz coils enable manipulation of the spin states via controlled application of magnetic-field pulses. The piercing solenoid is used both for guiding during shuttling and for generation of a tunable precession field inside the magnetic shield. **(C)** The typical experimental protocol uses a guiding magnetic field of 7µT inside the solenoid (proton precession frequency ~285Hz). Polarization in the 1T magnet lasted 5s for leaf samples and 10s for water calibration samples, followed by shuttling into the center of the magnetic shield within 100ms. A 30µT magnetic-field pulse was then immediately applied in order to rotate *z*-magnetization of the sample into the *x-y* plane (π/2 pulse), where subsequent free induction decay (FID) of the magnetization signal in the precession field was recorded by the magnetometers. Signal acquisition time was set to 2s for leaf samples and 3−10s for water calibration samples.

symmetrically around a magnetic dipole initialized along $-\hat{x}$ and undergoing Larmor precession clockwise in the plane at positive angular frequency ω_0, we can write the following (ideal) expressions for the oscillating magnetic field sensed by the four magnetometer channels as a function of time t:

$$B_{x_1}(t) = \mu_0\, m_0 \cdot \cos\,(\omega_0 t) \cdot e^{-t/T_2}/(4\pi r^3), \qquad (1)$$

$$B_{y_1}(t) = \mu_0\, m_0 \cdot \sin\,(\omega_0 t) \cdot e^{-t/T_2}/(2\pi r^3);$$

$$B_{x_2}(t) = -\mu_0\, m_0 \cdot \cos\,(\omega_0 t) \cdot e^{-t/T_2}/(2\pi r^3), \qquad (2)$$

$$B_{y_2}(t) = -\mu_0\, m_0 \cdot \sin\,(\omega_0 t) \cdot e^{-t/T_2}/(4\pi r^3).$$

Here, r is the offset distance of the center of the sensing volumes from the magnetic dipole (the sample is modeled as a uniformly magnetized sphere); T_2 is the characteristic exponential decay time of the precession signal; μ_0 is the vacuum permeability constant. Note the factor-of-two difference between pairs of measured field components; this is the result of a dipole-field geometry as measured by point-like sensors. The initial magnetic-moment amplitude m_0 equals the sample volume times the magnetization of the sample. Note that each measured magnetic-field component may be positive or negative, since vector rather than scalar magnetometers are used. For a spherical 1mL sample of water polarized at 1T and room temperature (typically 22°C in our lab), one can estimate magnetic-field values (at the beginning of the measurement assuming no

relaxation losses) on the order of 100pT, given the experimental offset distance of 17.5mm. This agrees with experimental data (Figure 2); a complete calculation is provided in Supplementary Material. We note that, fundamentally, Equations 1, 2 should contain T_2^* rather than T_2, as we do not employ CPMG or other dynamic decoupling sequences to suppress effects of magnetic-field inhomogeneities at the position of the sample during measurement. However, because the studied leaf samples have intrinsically high relaxation rates (T_2 of 150–300ms, see Section 3) which are larger than contributions due to inhomogeneity of the solenoid (Figure S8), such simplification is warranted in our case.

We see from Equations 1, 2 and the geometry in Figure 1A that by subtracting the measured fields along the x- and y-axes, respectively, the signals along each axis add—leading to a signal enhancement of 1.5, assuming identical sensor response—while common-mode noise is canceled. Furthermore, the two gradiometric signals have a relative phase of $\pi/2$—i.e., are in-quadrature—which becomes useful for signal processing in the frequency domain via Fourier transform. This is the basis of what we have termed the "gradiometric quadrature" detection scheme, used in the work reported here to achieve enhanced (by a factor of ~3 compared to single-channel measurement) proton signals in *ex vivo* tree leaves.

The experimental setup, contained in a portable instrument rack, is depicted schematically in Figure 1B. Thermal polarization of nuclear spins is created using a 1T Halbach magnet with 15mm bore, which defines the maximum possible diameter of measured samples. After adequate polarization-buildup time in the magnet (5–10s), rapid (~100ms) mechanical shuttling of the sample into

the magnetic shield (Twinleaf MS-1LF) is performed using an Arduino-controlled stepper motor driving a plastic gear rack, to which a nonmagnetic sample holder is attached. Shuttling occurs inside a double-layer piercing solenoid wrapped around a plexiglass tube and reaching from the top of the Halbach magnet through the magnetic shield. At the center of the shield, a 3D-printed frame of ABS plastic contains three pairs of Helmholtz coils (radius 33mm) for creation of magnetic-field pulses along the x-, y-, or z-axes to manipulate the nuclear-spin state, as well as two atomic magnetometers (QuSpin QZFM Gen-2) for detection of nuclear-spin signals (Figure 1A). These zero-field sensors can operate in ambient magnetic fields of up to tens of nT, which is readily achieved with the magnetic shield, with the aid of built-in compensation coils. We introduced the piercing solenoid specifically to be able to separate the background field on the sensors from the precession field on the sample. A field on the order of 10μT may be generated inside the piercing solenoid without compromising sensor operation, as field leakage outside the solenoid is usually below 1%. The range of achievable precession frequencies is ultimately limited by sensor bandwidth—below 500Hz for the atomic magnetometers used in this work.

Figure 1B shows the typical relaxometry protocol for the experiments reported here. After spin polarization and shuttling, immediate application of a $\pi/2$-pulse in the y-direction rotates the bulk z-magnetization into the x-axis, where it subsequently precesses about the leading z-field of amplitude B_0 at an angular frequency ω_0 given by the proton gyromagnetic ratio γ_{1_H} according to $\omega_0 = \gamma_{1_H} B_0$, where $\gamma_{1_H}/2\pi \approx 43\text{Hz}/\mu\text{T}$. This Larmor precession gives rise to a free-induction-decay (FID) signal which is acquired
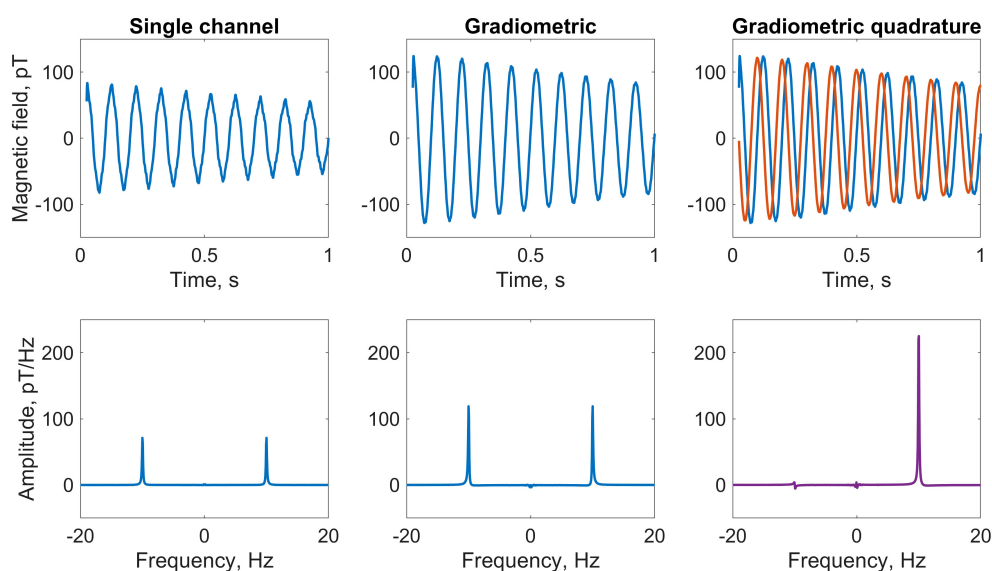

FIGURE 2
Comparison of water-proton NMR calibration spectra using three different detection modalities. A 1.5mL vial of deionized water was measured using the detection geometry and relaxometry protocol depicted in Figure 1, at a 230nT (10Hz) precession field. Plots show the average of four scans. Top row, left to right: first second of the free-induction-decay (FID) signal recorded by the y-channel of sensor 1; gradiometric FID signal (difference of signals from the y-channels of sensors 1 and 2), showing signal enhancement and noise suppression; overlaid x (red) and y (blue) gradiometric FID signals, which are summed in quadrature as described in the text. Bottom row: corresponding frequency spectra obtained by fast Fourier transform (FFT); the signal at +10Hz is enhanced at least 2.5 times in the phased quadrature spectrum (rightmost panel) as compared to a phased single y-channel spectrum (leftmost panel). Only a small residual remains at −10Hz due to imperfections in the quadrature geometry, after correcting for differences in gain of the gradiometric channels. For plotting, a 50Hz low-pass filter was applied to the data in the time domain.

by the magnetometers. For proton spins (positive sign of the gyromagnetic ratio), precession is "left-handed", occurring clockwise about the applied magnetic field (Levitt, 1997).

Experimental timing and control as well as detector readout were implemented in Labview using NI TTL-pulse and data-acquisition cards. To maximize the SNR of the measured FID signal, a number of experimental parameters were iteratively optimized. These include: polarization time, solenoid field (proton precession frequency), shuttling time and speed/acceleration, pulse duration and amplitude, and acquisition time. Various calibration data, along with photos and further details of the apparatus, may be found in Supplementary Material.

2.2 Data processing

During acquisition of an FID according to the protocol in Figure 1B, the analog voltage outputs of all four magnetometer channels are recorded at a user-defined sampling rate, usually 2kHz, for subsequent analysis. Although the sensors are always calibrated (i.e., ambient magnetic fields internally compensated) with the sample in the measurement position prior to each experiment, application of the magnetic-field pulse drives the sensors out of their sensitive range for some tens of milliseconds. Thus, initial data points must be discarded in post-processing, resulting in an effective linear phase shift of the recorded oscillating signal. Because each magnetometer channel provides a vector measurement—sensitive to the sign of the magnetic field, in contrast to a scalar sensor—the handedness of spin precession may be deduced from a single-channel time trace, if it is possible to reconstruct the true phase of the FID. However, the quadrature detection scheme allows us to determine the handedness without having to reconstruct the phase.

As an illustration of the analysis procedure, Figure 2 shows calibration data from a liquid water sample at a proton precession frequency of 10Hz, obtained by supplying a current of 54μA to the piercing solenoid. The first 25ms of data, corresponding to the first 50 points of the FID sampled at 2kHz, have been discarded to remove post-pulse artifacts which would otherwise adversely affect the spectral lineshape and baseline (the calibrated magnetometers have a dynamic range of approximately 5nT; the applied pulse of 30μT prior to acquisition temporarily pushes them out of range). Plots show the average of multiple (here, four) scans, where a linear trend has been removed from each individual raw time trace prior to averaging. This detrending of time-domain signals mitigates the effect of low-frequency magnetic-field drifts in the lab environment, which may negatively impact spectral baselines in the frequency domain. Initially, we convert from voltage to magnetic-field units to obtain four time series associated with the four magnetometer channels, which we denote x_1, y_1, x_2, and y_2, following Equations 1, 2. The two gradiometric channels are subsequently constructed as $x = x_1 - x_2$ and $y = y_1 - y_2$. By examining the single-channel and gradiometric time traces in the context of the detection geometry (Figure 1A), we can confirm that the spin signal was initialized along $-\hat{x}$ and is precessing clockwise in the x-y plane, consistent with a precession field along $+\hat{z}$. Furthermore, reduction of higher-frequency noise via gradiometry is visible.

The gradiometric-quadrature channel can be constructed from the two gradiometric channels as $x+iy$ (see Supplementary Material for more details). In our experimental geometry, the time-dependent quadrature signal may be thought of as a vector rotating clockwise in the complex plane defined by a real x-axis and imaginary y-axis. Assuming perfect quadrature geometry, when a standard Fourier transform is performed to convert the signal into the frequency domain, the resulting spectrum should contain a resonance only at +10Hz and not at −10Hz.

In the time domain, the processed complex gradiometric-quadrature signal is written as

$$S(t) = e^{i\phi}[a \cdot x(t) + ib \cdot y(t)], \qquad (3)$$

where $x(t)$ and $y(t)$ are the gradiometric signals, and ϕ is an overall phase selected such that the real part of the frequency spectrum has an absorptive peak (see below) (Keeler, 2010). The numerical coefficients a and b are defined so that $a + b = 2$, and may be adjusted to account for possible differences in gain between the two channels—usually a few percent or less, based on suppression of the residual negative-frequency peak. Prior to the Fourier transform, zeros may be added to the end of the time series defined by Equation 3 (zero-filling) in order to increase the spectral resolution.

All frequency spectra throughout this manuscript are plotted such that the y-axis has units of pT/Hz or fT/Hz, depending on the signal strength. These units arise from the discrete Fourier transform (DFT) used to convert data from the time domain to the frequency domain and subsequent data processing, as explained in detail in Supplementary Material.

The exact SNR enhancements attainable by the gradiometric quadrature method depend strongly on performance of the individual sensors, which may vary between experiments, as well as non-common-mode systematic noise. In our experience with water calibration samples, compared to single-channel spectra, SNR could be enhanced up to 75% via gradiometry alone and up to 300% via the gradiometric quadrature method (depending on sensor performance). This indicates not only that gradiometry is effective in terms of noise suppression, but also that the quadrature approach is more beneficial than simply summing the positive-frequency and negative-frequency peaks in a traditional "mirrored" non-quadrature spectrum. See Supplementary Material for quadrature simulations, gradiometer sensitivity data, and further details about phasing of quadrature signals. We expect that gradiometric quadrature detection can be especially advantageous for situations in which sensitive magnetometers operate in unshielded environments—if the contribution from common-mode noise dominates the contribution from uncorrelated noise at the positions of two sensors, total measurement noise will be significantly suppressed.

2.3 Leaf harvest and sample preparation

A description of all 19 tree-leaf samples included in our study is provided in Table 1. For identification purposes, samples from each genus were numbered in order of preparation/measurement date. We note that, due to seasonal availability, evergreen (spruce, pine,

TABLE 1 Overview of the leaf measurement campaign, in which samples from seven different tree genera were studied.

Genus	Species/cultivar	Sample	Date measured, 2023-MM-DD	Leaf mass, ± 1mg	Signal amplitude, fT/Hz	T_2, ms
spruce (Picea)	Norway spruce (*Picea abies*) "Acrocona"	S1	02-24	592	68.3 ± 2.2	197 ± 2
			02-27	520	26.7 ± 0.9	158 ± 2
			03-08	344	2.5 ± 0.5	164 ± 13
		S2	02-25	648	53.3 ± 2.1	151 ± 2
			02-28	590	27.0 ± 0.6	162 ± 2
			03-13	322	0.9 ± 0.7	290 ± 83
	Norway spruce (*Picea abies*)	S3	03-02	664	30.0 ± 1.1	193 ± 3
			03-04	592	11.7 ± 0.7	182 ± 4
			03-14	393	2.2 ± 0.8	258 ± 37
		S4	03-03	714	34.9 ± 3.3	310 ± 11
			03-07	616	27.4 ± 1.7	295 ± 7
			03-16	414	1.4 ± 0.7	296 ± 57
pine (Pinus)	mountain pine (*Pinus uncinata*)	P1	03-09	1001	10.2 ± 1.0	196 ± 7
		P2	03-10	516	13.1 ± 0.8	173 ± 4
	dwarf mountain pine (*Pinus mugo*)	P3	03-17	512	26.3 ± 1.9	324 ± 9
		P4	03-20	503	22.5 ± 1.5	264 ± 7
yew (Taxus)	common yew (*Taxus baccata*)	Y1	03-22	596	4.5 ± 0.6	191 ± 10
		Y2	04-06	690	3.3 ± 0.5	182 ± 10
hazel (Corylus)	common hazel (*Corylus avellana*)	H1	04-04	404	5.2 ± 0.7	193 ± 10
		H2	04-07	584	9.8 ± 0.7	209 ± 6
		H3	04-10	682	19.2 ± 1.2	262 ± 6
cherry (Prunus)	bird cherry (*Prunus padus*)	C1	04-11	525	23.7 ± 3.9	223 ± 14
		C2	04-12	504	34.7 ± 5.1	189 ± 11
beech (Fagus)	European beech (*Fagus sylvatica*) "Rohanii"	B1	05-04	463	48.6 ± 3.4	259 ± 7
		B2	05-05	446	44.2 ± 4.3	355 ± 13
oak (Quercus)	pubescent oak (*Quercus pubescent*)	O1	05-17	932	70.3 ± 3.1	222 ± 4
			05-23	738	2.8 ± 0.8	348 ± 38
			05-30	721	3.5 ± 0.8	396 ± 33
		O2	05-19	531	36.0 ± 2.9	233 ± 7
			05-25	323	2.3 ± 1.0	536 ± 93
			05-31	254	4.1 ± 1.4	563 ± 75

Branchlets were freshly harvested in the Mainz Botanical Garden and transported to the lab in a beaker of distilled water for immediate sample preparation and measurement. Intact leaves were carefully dried and packed into a 2mL closed glass vial, which was weighed and inserted into the experimental apparatus for a 13h measurement (4096 scans). For dehydration studies (spruce and oak), sample vials were stored uncapped between measurements in a plant growth chamber at 22°C.

and yew) leaves were collected from late February to early April, while deciduous (hazel, cherry, beech, and oak) leaves were collected from early April to late May. Sample collection occurred as close as possible to the time of first measurement. All samples were sourced from the Eurasian arboretum of the Mainz Botanical Garden, which informed the specific choice of species and/or cultivar, although we purposely selected a diverse range of common genera.

During harvest, a branchlet containing sufficient leaf coverage was cut from the branch tip of the tree donor and immediately placed in a glass beaker partially filled with distilled water such that the cut end of the branchlet was submerged, as shown in the photo

inset of Figure 3. Sample preparation in the laboratory proceeded as follows. Leaves or needles were gently removed from the branchlet, thoroughly dried with a clean tissue to remove any excess moisture, and packed into a pristine glass shell vial (BGB SV2ML) with outer diameter 11.6mm and interior volume 3.3cm^3. Spruce, pine, and yew needles were placed lengthwise vertically into the vial, whereas the hazel, cherry, beech, and oak leaves had to be rolled or folded. Care was taken to avoid tearing or otherwise damaging leaves during sample preparation, thereby preserving the original structure of the plant tissue, while fitting as many leaves or needles as possible into the tubular vial (Figure 3 photo inset). Due to leaf geometry, it was not possible to achieve completely
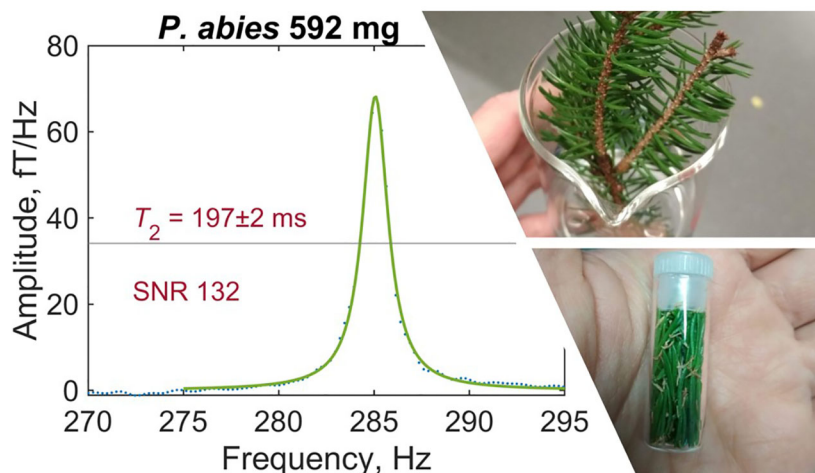
FIGURE 3
Example of a typical leaf spectrum recorded by gradiometric quadrature detection (spruce sample S1). Water-proton signal has been fitted with a Lorentzian and phased such that fit residuals are minimized—see text for details of data analysis. Inset photos show a freshly harvested spruce branchlet (top) and a prepared sample of spruce needles (bottom).

uniform density of leaf material in the vial, particularly for larger deciduous leaves. Each individual vial and its plastic cap were weighed with a digital scale before and after leaf insertion to extract the total leaf mass. Vials were capped prior to and throughout each 13h experiment in the relaxometry setup, to prevent dehydration of the sample. After each experiment, the capped vial was removed from the setup, uncapped to release any trapped water vapor, recapped and weighed again. We found that post-measurement mass was always within a few mg of pre-measurement mass (Table 1), suggesting that leaf dehydration during the experiment was negligible, and that little to no excess water vapor had been contained inside the vial.

For the dehydration investigation, one evergreen genus (spruce) and one deciduous genus (oak) were selected; each sample was measured three different times, on the dates indicated in Table 1. Between experiments, the sample vial was stored uncapped in an on-site plant growth chamber (poly klima PK-520, 22°C, 12/12 h light/dark cycle, no humidity control). Because the vial was open only at one end, uniform dehydration of the leaf content could not be ensured. However, visible inspection of leaf color as well as the usual weighing procedure indicated that water loss had occurred during each storage period. It was critical to ensure that no condensation collected inside the vials at any stage of dehydration or measurement preparation, as this could introduce an additional spurious water-proton signal (sharp peak due to free water) not originating from water protons contained in the leaves themselves.

2.4 Leaf measurements

Each leaf measurement was conducted under identical experimental conditions to produce a proton-NMR spectrum as in Figure 3. A resonance frequency of around 285Hz, corresponding to a 7μT precession field with 1.5mA applied to the piercing solenoid, was selected to avoid lower-frequency noise while

remaining with the sensitive bandwidth of the magnetometers (see Supplementary Material). In the plotted spectrum, linear background was removed in the region 260–320Hz and a Lorentzian fit (three-parameter Lorentzian function with constant term) was performed using the *lorentzfit* script in Matlab. As expected, the experimental lineshape is well-fitted by a Lorentzian, as it results from an exponentially decaying signal. Phasing of the quadrature signal was optimized by minimizing the root mean square error (RMSE) of the fit. Using the calculated fit parameters and errors thereon, the fit amplitude and linewidth (FWHM, full width at half maximum) were extracted. Typical fit amplitudes were on order 1 to 10fT/Hz—at least three orders of magnitude smaller than for pure water samples of similar volume—after averaging over 4096 scans (repetitions of the measurement protocol). The relaxation time T_2 is related to the FWHM Δ as $1/(\pi\Delta)$. Reported SNR values were obtained from the ratio of fit amplitude to the standard deviation of spectral noise in the region 265–275Hz. To avoid artificial broadening of the spectral line, no apodization was used; instead, a 300Hz low-pass filter was applied to each spectrum for lineshape correction of the averaged signal. Measured proton-signal amplitudes and T_2 times are recorded for all 35 leaf experiments in Table 1. Complete fitted spectra, along with example analysis code and further details of the analysis protocol, may be found in Supplementary Material.

In principle, multiple mechanisms may affect the spectral linewidth. These include magnetic-field gradients at the location of the sample, combined effects of different relaxation mechanisms, and possible contributions from non-water protons. Due to the significant differences in linewidth between liquid and leaf samples, we conclude that field inhomogeneity at the location of the sample is negligible, and therefore we report T_2 rather than T_2^* times in this work. As described in Section 2.2, the dead time required before data acquisition places a lower limit of 25ms on measurable T_2 times, which is acceptable for studies of free or loosely bound water protons. Because experimental parameters remained unchanged

over the course of the leaf study and all data underwent an identical analysis procedure, direct comparison of signal amplitudes and T_2 times is possible. Comparing the leaf results to typical water calibration data, we find that T_2 times in fresh leaf samples are an order of magnitude shorter than in liquid water samples of similar volume.

3 Results

Figures 4, 5 provide graphical representations of the results reported in Table 1. In Figure 4A, we see that the normalized signal amplitude of the spectra obtained from freshly prepared leaf samples varies significantly by tree genus. This may indicate different water-storage capacities of leaves from different genera. It is interesting to note that packing more leaf matter into the sample vial to increase the overall sample mass did not necessarily increase the normalized signal amplitude, for leaves of the same species. This could be attributed to two effects: (1) non-uniformity of the packing of leaf matter inside vials and (2) demagnetization effects due to the fact that samples are cylindrical rather than spherical. Due to leaf shape, distribution of leaf material in the sample vial is not necessarily uniform and this is generally worse for deciduous trees than for evergreen trees, due to the needle-like form of the latter. We observe that evergreen tree leaves fill up vials more uniformly. Demagnetization field effects due to cylindrical sample geometry can result in lowered signal for some samples compared to others (Table 1). Future studies are warranted to investigate the effects of sample geometry and uniformity of leaf matter on the magnitude of observable NMR signals and the precise amount of water giving rise to them. In contrast to the amplitude results, we see from Figure 4B that average measured T_2 times do not appear to vary significantly among the studied tree genera.

In Figure 5, showing the results of the spruce/oak dehydration study, two trends can be observed. First, we observe an overall decrease in signal amplitude as sample mass decreases due to water loss, indicating that our experiments are primarily sensitive to water protons, as expected. However, we note that the dependence on

sample mass is not entirely linear—this may be related to inhomogeneous dehydration of the sample, as mentioned above, as well as possible signal contributions from non-water protons. Second, an overall increase of T_2 times, i.e. narrowing of the water-proton peak, is observed as sample mass decreases. This trend is more pronounced for the oak samples, even accounting for increased uncertainty on T_2 due to reduction of SNR with dehydration. Notably, T_2 increases most dramatically for oak samples, as compared to spruce.

4 Discussion

In this study, we showcased several key findings, including the noninvasive and nondestructive measurement of water signals in intact *ex vivo* plant parts using a proton relaxometry protocol at hypogeomagnetic field. Additionally, we achieved signal-to-noise ratio enhancement of weak biological NMR signals from non-solution samples by employing a gradiometric quadrature detection scheme, especially useful in a future deployment of this technology in the field. Our research involved a comparative investigation of water-proton signals and T_2 relaxation in 19 tree-leaf samples, encompassing samples from seven genera, eight species, and nine cultivars. With this, we demonstrated sensitivity to the evolution of water-proton signals and T_2 relaxation times through repeated measurements of dehydrating leaf samples.

The experiments reported here were intended as a proof-of-principle of the above, and have not yet attempted to answer specific biological questions. Nonetheless, the preliminary results displayed in Figures 4, 5 already contain information which suggests future lines of relaxometry research with tree leaves. For example, the observed differences in normalized water-proton signal amplitude among different genera and species/cultivars may motivate further large-sample-size studies of water-storage capacity and possible seasonal variations. By contrast, the relative uniformity of measured T_2 times in all fresh leaf samples indicates that, at least in the hypogeomagnetic field regime, water-proton relaxation in leaf tissue is dominated by mechanisms common to the studied tree types. The observed
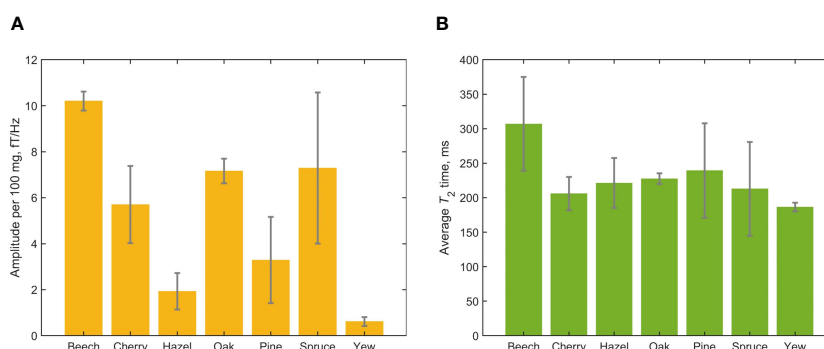

FIGURE 4
Results of the cross-species leaf-relaxometry study encompassing 19 fresh leaf samples. **(A)** Average normalized measured water content from the different tree genera. Signal amplitudes were extracted from Lorentzian fits of the measured spectra; error bars indicate the standard deviation of signal amplitude for each genus. Note that the spruce and pine data encompass multiple species or cultivars (Table 1). **(B)** Average T_2 times, extracted from Lorentzian fits of the measured spectra; error bars indicate the standard deviation for each genus.
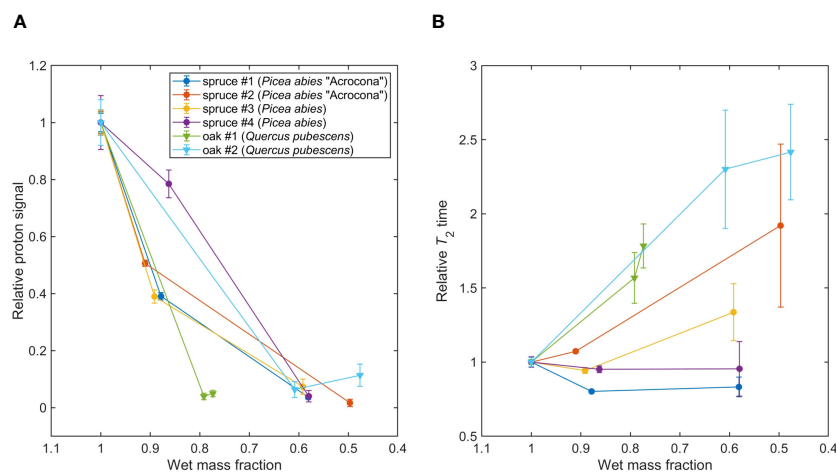
FIGURE 5

(A) Tracking water content with dehydration in spruce (*P. abies*) and oak (*Q. pubescens*) leaves, see Table 1. Signal amplitudes and errors were extracted from Lorentzian fit parameters of the measured spectra; lines connecting data points are a guide to the eye. **(B)** Tracking proton T_2 relaxation times with dehydration. Relaxation times and errors were extracted from Lorentzian fit parameters of the measured spectra; lines connecting data points are a guide to the eye.

tendency toward lengthening of T_2 times (narrowing of the proton precession peak) with leaf dehydration, particularly in the measured oak samples, may seem contradictory to intuition—if one expects dehydration and tissue death to further constrain molecular motion and lead to broadening of the spectral feature. However, our result appears to be consistent with previous benchtop relaxometry studies where leaf senescence was correlated with changes in water distribution at the cellular level as well as lengthening of T_2 components (Musse et al., 2013; Musse et al., 2017). Thus, we hope that our tree-leaf dehydration study will help open to the door to further relaxometry-enabled research on drought stress and tolerance in the context of forestry and agriculture.

Further improvements to the experimental setup will enable the affordable atomic-magnetometer based relaxometry device to achieve the functionality of commercial benchtop spectrometers for biological applications. These refinements may include implementation of spin-echo pulse sequences, SNR enhancements via suppression of low-frequency noise and optimization of the shuttling field profile, and shimming (field compensation) of stray magnetic fields and gradients. Relaxation-dispersion studies (measuring relaxation times as a function of field) may also reveal further information about water-storing structures (Brewer and Bhattacharyya, 1986; Rommel et al., 1988; Halle and Denisov, 2002). Instrumentation such as custom magnetometers tailored to plant samples—with reduced standoff distance and surface temperature—will improve biocompatibility, and the use of Earth-field magnetometers would even enable unshielded measurements (see (Fabricant et al., 2023) and references therein). The shielded regime is itself of fundamental interest, for example in studying properties of biological tissues under hypogeomagnetic conditions such as those encountered during long-distance spaceflight. Relaxometry studies of systems in which NMR signals originate from molecules other than water are also valuable, since other relaxation mechanisms can be

involved (Alcicek et al., 2023). While future experiments need not be limited to relaxometry of protons only, NMR-enabled investigation of plant water dynamics is highly warranted, particularly in ultralow and hypogeomagnetic regimes.

Data availability statement

The raw data supporting the conclusions of this article will be made available by the authors, without undue reservation.

Author contributions

AF: Conceptualization, Data curation, Formal Analysis, Investigation, Methodology, Software, Visualization, Writing – original draft, Writing – review & editing. PP: Investigation, Methodology, Software, Writing – review & editing. DB: Conceptualization, Funding acquisition, Investigation, Methodology, Resources, Supervision, Writing – review & editing.

Funding

Acknowledgments

Dr. Kirill F. Sheberstov, Liubov Chuchkova, Oleg Tretiak, and Dr. Raphael Kircher in initial development of the experimental setup. The Halbach magnet used for spin polarization was designed by Dr. Peter Blümler. We thank the Mainz Botanical Garden Arboretum for providing samples for this study.

Conflict of interest

The authors declare that the research was conducted in the absence of any commercial or financial relationships that could be construed as a potential conflict of interest.

Publisher's note

All claims expressed in this article are solely those of the authors and do not necessarily represent those of their affiliated organizations, or those of the publisher, the editors and the reviewers. Any product that may be evaluated in this article, or claim that may be made by its manufacturer, is not guaranteed or endorsed by the publisher.

Supplementary material

The Supplementary Material for this article can be found online at: https://www.frontiersin.org/articles/10.3389/fpls.2024.1352282/full#supplementary-material

References

Alcicek, S., Put, P., Kubrak, A., Alcicek, F. C., Barskiy, D., Gloeggler, S., et al. (2023). Zero- to low-field relaxometry of chemical and biological fluids. *Commun. Chem.* 6, 165. doi: 10.1038/s42004-023-00965-8

Araujo, C., MacKay, A., Hailey, J., Whittall, K., and Le, H. (1992). Proton magnetic resonance techniques for characterization of water in wood: Application to white spruce. *Wood Sci. Technol.* 26, 101–113. doi: 10.1007/BF00194466

As, H. V., and van Duynhoven, J. (2013). MRI of plants and foods. *J. Magnetic Resonance* 229, 25–34. doi: 10.1016/j.jmr.2012.12.019

Ates, E. G., Domenici, V., Florek-Wojciechowska, M., Gradišek, A., Kruk, D., Maltar-Strmečki, N., et al. (2021). Field-dependent NMR relaxometry for food science: Applications and perspectives. *Trends Food Sci. Technol.* 110, 513–524. doi: 10.1016/j.tifs.2021.02.026

Berns, A. E., Bubici, S., Pasquale, C. D., Alonzo, G., and Conte, P. (2011). Applicability of solid state fast field cycling NMR relaxometry in understanding relaxation properties of leaves and leaf-litters. *Organic Geochemistry* 42, 978–984. doi: 10.1016/j.orggeochem.2011.04.006

Blanchard, J. W., and Budker, D. (2016). Zero- to ultralow-field NMR. *eMagRes* 5, 1395–1410. doi: 10.1002/9780470034590.emrstm1369

Blanchard, J. W., Budker, D., and Trabesinger, A. (2021). Lower than low: Perspectives on zero- to ultralow-field nuclear magnetic resonance. *J. Magnetic Resonance* 323, 106886. doi: 10.1016/j.jmr.2020.106886

Bodenstedt, S., Mitchell, M. W., and Tayler, M. C. D. (2021). Fast-field-cycling ultralow-field nuclear magnetic relaxation dispersion. *Nat. Commun.* 12, 4041. doi: 10.1038/s41467-021-24248-9

Brewer, C. F., and Bhattacharyya, L. (1986). Specificity of concanavalin A binding to asparagine-linked glycopeptides. A nuclear magnetic relaxation dispersion study. *J. Biol. Chem.* 261, 7306–7310. doi: 10.1016/S0021-9258(17)38391-6

Capitani, D., Brilli, F., Mannina, L., Proietti, N., and Loreto, F. (2009). *In situ* investigation of leaf water status by portable unilateral nuclear magnetic resonance. *Plant Physiol.* 149, 1638–1647. doi: 10.1104/pp.108.128884

Espy, M., Matlashov, A., and Volegov, P. (2013). SQUID-detected ultra-low field MRI. *J. Magnetic Resonance* 229, 127–141. doi: 10.1016/j.jmr.2013.02.009

Fabricant, A., Iwata, G. Z., Scherzer, S., Bougas, L., Rolfs, K., Jodko-Władzińska, A., et al. (2021). Action potentials induce biomagnetic fields in carnivorous Venus flytrap plants. *Sci. Rep.* 11, 1438. doi: 10.1038/s41598-021-81114-w

Fabricant, A., Novikova, I., and Bison, G. (2023). How to build a magnetometer with thermal atomic vapor: A tutorial. *New J. Phys.* 25, 025001. doi: 10.1088/1367-2630/acb840

Halle, B., and Denisov, V. P. (2002). Magnetic relaxation dispersion studies of biomolecular solutions. *Methods Enzymology* 338, 178–201. doi: 10.1016/S0076-6879(02)38220-X

Hartwig, S., Albrecht, H. H., Scheer, H. J., Burghoff, M., and Trahms, L. (2013). A superconducting quantum interference device measurement system for ultra low-field nuclear magnetic resonance. *Appl. Magnetic Resonance* 44, 9–22. doi: 10.1007/s00723-012-0387-9

Huang, W., Reddy, G., Li, Y., Larsen, J., and Shi, P. (2020). Increase in absolute leaf water content tends to keep pace with that of leaf dry mass—Evidence from bamboo plants. *Symmetry* 12, 1345. doi: 10.3390/sym12081345

Jaeger, F., Grohmann, E., and Schaumann, G. E. (2006). 1H NMR relaxometry in natural humous soil samples: Insights in microbial effects on relaxation time distributions. *Plant Soil* 280, 209–222. doi: 10.1007/s11104-005-3035-4

Jain, P., Liu, W., Zhu, S., Chang, C. Y. Y., Melkonian, J., Rockwell, F. E., et al. (2021). A minimally disruptive method for measuring water potential in planta using hydrogel nanoreporters. *Proc. Natl. Acad. Sci.* 118, e2008276118. doi: 10.1073/pnas.2008276118

Jazbinsek, V., Thiel, G., Müller, W., Wübbeler, G., and Trontelj, Z. (2000). Magnetic detection of injury-induced ionic currents in bean plants. *Eur. Biophysics J.* 29, 515–522. doi: 10.1007/s002490000105

Keeler, J. (2010). *Understanding NMR Spectroscopy. 2 edn* (Chichester, U.K.: John Wiley & Sons, Ltd).

Khan, M. I. H., Wellard, R. M., Nagy, S. A., Joardder, M., and Karim, M. (2016). Investigation of bound and free water in plant-based food material using NMR T2 relaxometry. *Innovative Food Sci. Emerging Technol.* 38, 252–261. doi: 10.1016/j.ifset.2016.10.015

Krishnan, P., Singh, R., Verma, A., Joshi, D., and Singh, S. (2014). Changes in seed water status as characterized by NMR in developing soybean seed grown under moisture stress conditions. *Biochem. Biophys. Res. Commun.* 444, 485–490. doi: 10.1016/j.bbrc.2014.01.091

Levitt, M. H. (1997). The signs of frequencies and phases in NMR. *J. Magnetic Resonance* 126, 164–182. doi: 10.1006/jmre.1997.1161

Malone, M. W., Yoder, J., Hunter, J. F., Espy, M. A., Dickman, L. T., Nelson, R. O., et al. (2016). *In vivo* observation of tree drought response with low-field NMR and neutron imaging. *Front. Plant Sci.* 7. doi: 10.3389/fpls.2016.00564

McCain, D. C. (1995). Nuclear magnetic resonance study of spin relaxation and magnetic field gradients in maple leaves. *Biophys. J.* 69, 1111–1116. doi: 10.1016/S0006-3495(95)79985-4

Musse, M., Cambert, M., and Mariette, F. (2010). NMR study of water distribution inside tomato cells: Effects of water stress. *Appl. Magnetic Resonance* 38, 455–469. doi: 10.1007/s00723-010-0139-7

Musse, M., Franceschi, L. D., Cambert, M., Sorin, C., Caherec, F. L., Burel, A., et al. (2013). Structural changes in senescing oilseed rape leaves at tissue and subcellular levels monitored by nuclear magnetic resonance relaxometry through water status. *Plant Physiol.* 163, 392–406. doi: 10.1104/pp.113.223123

Musse, M., Leport, L., Cambert, M., Debrandt, W., Sorin, C., Bouchereau, A., et al. (2017). A mobile NMR lab for leaf phenotyping in the field. *Plant Methods* 13, 53. doi: 10.1186/s13007-017-0203-5

Nagata, A., Kose, K., and Terada, Y. (2016). Development of an outdoor MRI system for measuring flow in a living tree. *J. Magnetic Resonance* 265, 129–138. doi: 10.1016/j.jmr.2016.02.004

Osborne, J., Orton, J., Alem, O., and Shah, V. (2018). Fully integrated, standalone zero field optically pumped magnetometer for biomagnetism. *Proc. SPIE 10548 Steep Dispersion Eng. Opto-Atomic Precis. Metrology XI 10548G* 51. doi: 10.1117/12.2299197

Put, P., Pustelny, S., Budker, D., Druga, E., Sjolander, T. F., Pines, A., et al. (2021). Zero- to ultralow-field NMR spectroscopy of small biomolecules. *Analytical Chem.* 93, 3226–3232. doi: 10.1021/acs.analchem.0c04738

Rommel, E., Noack, F., Meier, P., and Kothe, G. (1988). Proton spin relaxation dispersion studies of phospholipid membranes. *J. Phys. Chem.* 92, 2981–2987. doi: 10.1021/j100321a053

Sala, R. G., Westgate, M. E., and Andrade, F. H. (2007). Source/sink ratio and the relationship between maximum water content, maximum volume, and final dry weight of maize kernels. *Field Crops Res.* 101, 19–25. doi: 10.1016/j.fcr.2006.09.004

Saura-Mas, S., and Lloret, F. (2007). Leaf and shoot water content and leaf dry matter content of Mediterranean woody species with different post-fire regenerative strategies. *Ann. Bot.* 99, 545–554. doi: 10.1093/aob/mcl284

Savukov, I., Seltzer, S., and Romalis, M. (2007). Detection of NMR signals with a radio-frequency atomic magnetometer. *J. Magnetic Resonance* 185, 214–220. doi: 10.1016/j.jmr.2006.12.012

Schnyder, H., and Baum, U. (1992). Growth of the grain of wheat (*Triticum aestivum* l.). The relationship between water content and dry matter accumulation. *Eur. J. Agron.* 1, 51–57. doi: 10.1016/S1161-0301(14)80001-4

Sorin, C., Mariette, F., Musse, M., Leport, L., Cruz, F., and Yvin, J. C. (2018). Leaf development monitoring and early detection of water deficiency by low field nuclear magnetic resonance relaxation in nicotiana tabacum plants. *Appl. Sci.* 8, 943. doi: 10.3390/app8060943

Tayler, M. C., Theis, T., Sjolander, T. F., Blanchard, J. W., Kentner, A., Pustelny, S., et al. (2017). Invited review article: Instrumentation for nuclear magnetic resonance in zero and ultralow magnetic field. *Rev. Sci. Instruments* 88, 091101. doi: 10.1063/1.5003347

Tayler, M. C., Ward-Williams, J., and Gladden, L. F. (2018). NMR relaxation in porous materials at zero and ultralow magnetic fields. *J. Magnetic Resonance* 297, 1–8. doi: 10.1016/j.jmr.2018.09.014

Trontelj, Z., Zorec, R., Jazbinsek, V., and Erné, S. (1994). Magnetic detection of a single action potential in *Chara corallina* internodal cells. *Biophys. J.* 66, 1694–1696. doi: 10.1016/S0006-3495(94)80960-9

Unal, K., Alpas, H., Aktas, H., and Oztop, M. H. (2020). Time domain (TD)-NMR relaxometry as a tool to investigate the cell integrity of tomato seeds exposed to osmotic stress (OS), ultrasonication (US) and high hydrostatic pressure (HHP). *J. Food Sci. Technol.* 57, 3739–3747. doi: 10.1007/s13197-020-04406-5

Windt, C. W., Nabel, M., Kochs, J., Jahnke, S., and Schurr, U. (2021). A mobile NMR sensor and relaxometric method to non-destructively monitor water and dry matter content in plants. *Front. Plant Sci.* 12. doi: 10.3389/fpls.2021.617768